

# Hole-Buffer Material Derived from Pyrene, Schiff Base and Tris to Enhance Emission Efficiency of Polymer Light-Emitting Diodes

Jyun-Huei Liou, Ping-Feng Hsu, Yun Chen\*

Department of Chemical Engineering, National Cheng Kung University, Taiwan

Email: \*yunchen@mail.ncku.edu.tw

**How to cite this paper:** Liou, J.-H., Hsu, P.-F. and Chen, Y. (2018) Hole-Buffer Material Derived from Pyrene, Schiff Base and Tris to Enhance Emission Efficiency of Polymer Light-Emitting Diodes. *Journal of Materials Science and Chemical Engineering*, 6, 31-46.

<https://doi.org/10.4236/msce.2018.63003>

**Received:** January 31, 2018

**Accepted:** March 17, 2018

**Published:** March 20, 2018

Copyright © 2018 by authors and Scientific Research Publishing Inc. This work is licensed under the Creative Commons Attribution International License (CC BY 4.0).

<http://creativecommons.org/licenses/by/4.0/>



Open Access

## Abstract

Inserting a hole-buffer layer is an effective way to enhance emission efficiency of electroluminescence devices. We have successfully synthesized a new hole-buffer material **PSB** composed of pyrene, Schiff base and trihydroxy *tert*-butyl groups by the Suzuki-coupling reaction. The HOMO and LUMO levels were  $-6.33$  eV and  $-2.55$  eV, respectively, as estimated from cyclic voltammograms. In addition, homogeneous films (rms roughness  $\sim 2$  nm) were readily obtained by spin-coating process. Multilayer polymer light-emitting diodes, ITO/PEDOT:PSS/**PSB**/SY/LiF/Al, have been fabricated using **PSB** as hole-buffer layer (HBL). Inserting **PSB** as HBL significantly enhances the performance (maximum luminance:  $26,439$  cd/m<sup>2</sup>, maximum current efficiency:  $7.03$  cd/A), compared with the one without **PSB** ( $9802$  cd/m<sup>2</sup>,  $2.43$  cd/A). It is also superior to the device with conventional BCP as hole-blocking layer (ITO/PEDOT:PSS/SY/BCP/LiF/Al:  $15,496$  cd/m<sup>2</sup>,  $5.56$  cd/A). Current results strongly indicate that the **PSB** is a potential hole-buffer material for electroluminescent devices.

## Keywords

Hole-Buffer, Polymer Light-Emitting Diodes, Pyrene, Schiff Base, Spin-Coating

## 1. Introduction

Organic light-emitting diodes (OLEDs) and polymer light-emitting diodes (PLEDs) have attracted considerable attention from both academic and industrial points of view due to promising applications in flat panel displays and solid-state lightings [1] [2] [3]. Device efficiency of OLEDs and PLEDs depend

mainly on the recombination ratio of holes and electrons injected from anode and cathode, respectively. Balance in holes and electrons (high carriers' recombination ratio) is crucial in enhancing device emission efficiency [4] [5] [6]. However, hole mobility in most organic materials is higher than electron mobility [6]; moreover, the injection rate of holes for most OLED/PLED devices is greater than that of electrons. This leads to imbalanced carriers and reduced device efficiency. Carriers balance can be improved by multilayer device structure, *i.e.*, inserting electron injection and transport layers between emission layer and the cathode [7] [8]. In this way, the injection and transport of electrons are raised to a level comparable to those of holes, resulting in more balanced carriers. Another effective strategy is to insert a hole-blocking layer between emissive layer and electron injection layer, such as bathocuproine (BCP), 2,2',2''-(1,3,5-benzinetriyl)-tris(1-phenyl-1-H-benzimidazole)(TPBi) and 1,3,5-tri(m-pyridin-3-ylphenyl) benzene (TmPyPB). The hole-blocking layer effectively confines the holes and excitons within the emissive layer due to its low HOMO level [9] [10] [11] [12]. Although this hole-blocking effect can accumulate holes within emissive layer to increase recombination ratio, the recombination region is usually a narrow zone close to the hole-blocking layer. The formation of excitons too near the interface usually leads to diminished color purity and emission efficiency [13].

Recently, hole-buffering materials have been developed to increase the recombination ratio and emission efficiency. The hole-buffering materials effectively reduce the mobility of holes, instead of increasing injection/transport of electrons, to raise the recombination ratio of carriers. For instance, copper (II) phthalocyanine (CuPC), and 4,4',4''-tris (N-carbazoyl)-triphenylamine (TATC) were deposited as hole-buffering layer which effectively reduced hole mobility [14] [15]. We have designed a polymer **3P<sub>5</sub>O** composed of alternating *p*-terphenyl and tetraethylene glycolether segments and successfully employed as hole-bufferlayer to improve carriers balance [16]. The hole buffer layer was inserted between hole injection and emissive layers, it reduces the mobility of holes and thus recombine with electrons in the whole emissive layer, leading to enhanced device performance [16] [17]. In 1999, Forsythe found that transport of holes from ITO anode to NPB hole-transporting layer was injection-limited and device performance depended on hole current [18]. They inserted different thickness of CuPC (0 - 30 nm) to reduce hole-injection into the emissive layer and effectively enhanced device performance. However, the CuPC layer should be formed by vacuum thermal deposition, whose disadvantages are high cost of fabrication processes and difficulty in fabricating large-area devices than solution process [19] [20]. In solution process, polymers are usually used because of their excellent film-forming property. Although this advantage makes polymers very appropriate for PLEDs, some inherent difficulties are still existed for polymers applied in PLEDs, such as purification, control of batch-to-batch variations and wide distribution of molecular weight. On the contrary, the advantages of small

molecules applicable in solution process are exact molecular structure and high purity. However, some problems may emerge when applied to device fabrication using solution processes, such as limited film-forming property and poor morphology in film state [20].

In this study, we have designed and successfully synthesized a new small molecular hole-buffering material **PSB** by the Suzuki-coupling reaction. The core of **PSB** is a pyrene symmetrically attached with two phenol groups, from which imine (Schiff base) and trihydroxy *tert*-butyl groups are linked. The pyrene core is introduced to raise hole transport ability [21]; however it aggregates readily due to its flat structure [22]. The aggregation may cause aggregation or crystallization during device operation, which becomes as defect in PLEDs to reduce device efficiency and life times. To solve this problem, bulky trihydroxy *tert*-butyl groups are introduced to prevent aggregation by steric hindrance. Moreover, **PSB** is inserted with imine linkage (Schiff base) between phenol and trihydroxy *tert*-butyl groups. The electron-withdrawing propensity of imine moiety is expected to slow down hole-transporting rate. In addition, homogeneous film of **PSB** was readily obtained by solution process. Multilayer OLED devices were fabricated by using **PSB** as hole-buffering layer [ITO/PEDOT:PSS/PSB/SY/LiF/Al]. The optimal performance of **PSB**-based device (maximum luminance: 26,439 cd/m<sup>2</sup>, maximum current efficiency: 7.03 cd/A) is much better than the one without **PSB** [ITO/PEDOT:PSS/SY/LiF/Al] (9,802 cd/m<sup>2</sup>, 2.43 cd/A). Furthermore, the performance also surpasses the device with conventional BCP as hole-blocking layer [ITO/PEDOT:PSS/SY/BCP/LiF/Al] (15,496 cd/m<sup>2</sup>, 5.56 cd/A). Apparently, the hole-buffering property of **PSB** is effective in enhancing emission efficiency of electroluminescent devices.

## 2. Materials and Methods

### 2.1. General Procedures

Thermal degradation and transition behaviors of the **PSB** were investigated using thermogravimetric analysis (TGA) and differential scanning calorimetry (DSC), respectively. The TGA was conducted under a nitrogen atmosphere, heated from ambient temperature to 580°C at a rate of 10°C/min using a PerkinElmer TGA-7 thermal analyzer. The thermal decomposition temperature ( $T_d$ ) was determined at 5% weight loss of the sample. The thermal transitional properties were measured from -100°C to 260°C under a nitrogen atmosphere, using a DSC 2010 from TA Instruments. The glass transition temperature ( $T_g$ ) was determined from the second heating scan. Cyclic voltammograms (CVs) were measured with a voltammetric apparatus (model CV-50W from BAS) equipped with a three-electrode cell. The cell was made up of a glassy carbon as the working electrode, an Ag/AgNO<sub>3</sub> electrode as the reference electrode, and a platinum wire as the auxiliary electrode. The electrodes were immersed in acetonitrile containing 0.1 M (*n*-Bu)<sub>4</sub>NClO<sub>4</sub> as the electrolyte. The energy levels were calculated using the ferrocene (FOC) value of -4.8 eV with respect to vacuum level,

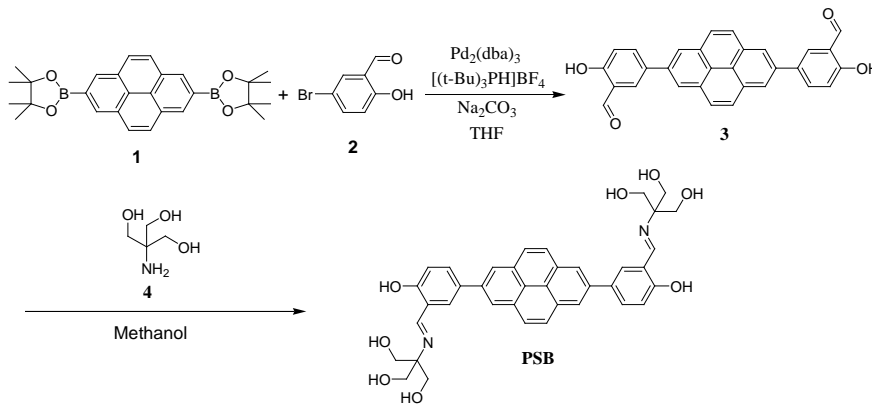
which is defined as zero. Absorption and photoluminescence (PL) spectra were measured with a Jasco V-550 spectrophotometer and a Hitachi F-4500 fluorescence spectrophotometer, respectively. The surface morphologies of deposited films were measured with an atomic force microscope (AFM), a Dimension Icon from Bruker. The film thickness was measured with a surface profilometer (Surfcorder ET4000 M).

## 2.2. Synthesis of PSB [23]

The synthetic routes of the pyrene derivative **PSB** are shown in **Scheme 1**. To a sodium carbonate solution (0.6 M, 2.8 mL) in 50-mL glass reactor was added with 2, 7-bis (4,4,5,5-tetramethyl-1,3,2-dioxaborolan-2-yl) pyrene (**1**: 0.2 g, 0.44 mmol), 5-bromo-2-hydroxybenzaldehyde (**2**: 0.264 g, 1.32 mmol), and tri-*tert*-butylphosphonium tetrafluoroborate (0.032 g, 0.11 mmol). The solution of tris (dibenzylideneacetone) dipalladium (0) ( $\text{Pd}_2(\text{dba})_3$ ; 57 mg, 0.06 mmol) in THF (18 mL) was added into the reactor by a syringe. The mixture was stirred at 65 °C for two days to afford 5,5'-(pyrene-2, 7-diyl)bis(2-hydroxybenzaldehyde) (**3**). A mixture of **3** (0.15 g, 0.39 mmol), 2-amino-2-(hydroxymethyl) propane-1, 3-diol (**4**: 0.41 g, 3.9 mmol) and methanol (150 mL) was stirred at 65 °C for two days. The methanol was removed by a rotary evaporator to obtain a crude product, which was further washed thoroughly with water and acetone several times to obtain **PySb** (yield: 0.20 g, 90.8%). The structure of **3** and **PSB** have been successfully confirmed by  $^1\text{H}$  NMR and elemental [23].

## 2.3. Devices Fabrication and Measurements

ITO glass substrates were cleansed successively, in an ultrasonic cleaner, with neutral detergent, deionized water, acetone, and isopropyl alcohol at 45 °C, each for 20 min. Then the substrates were further treated in a UV-ozone chamber for 20 min to remove trace organic contaminants. A solution of PEDOT:PSS was spin-coated onto the ITO surface to deposit the hole-injection layer, followed with baking at 140 °C for 20 min. Next, a **PSB** solution in N, N-dimethylformamide (DMF) was spin-coated on top of the PEDOT:PSS layer to form as hole-buffering



**Scheme 1.** Synthetic procedures of pyrene-Schiff base derivative **PSB**.

layer, followed by annealing at 70°C for 20 min. The emission layer was spin-coated from a toluene solution of Super Yellow (SY, Merck), followed with annealing at 70°C for 20 min. Finally, the substrate was transferred into a vacuum chamber to deposit LiF (1 nm) as an electron injection layer and then aluminum (90 nm) as the cathode, at a pressure less than  $2 \times 10^{-6}$  Torr. Finally, current density-voltage-brightness (J-V-L) characteristics of the devices were recorded using a combination of a Keithley power source (model 2400) and an Ocean Optics usb2000 fluorescence spectrophotometer.

### 3. Results and Discussion

#### 3.1. Thermal, Photo-Physical and Electrochemical Properties

Thermal decomposition behavior of **PSB** was investigated by thermogravimetric analysis under nitrogen atmosphere, between room temperature and 580°C. As shown in **Figure 1**, the thermal degradation of **PSB** is a two-stage process, including a quick weight loss at about 300°C and a slow degradation between 300°C and 580°C. The first quick weight loss is attributable to thermal decomposition of terminal imine and trihydroxy *tert*-butyl groups, whereas the latter slow degradation should be caused by the decomposition of aromatic chromophores. The thermal decomposition temperature ( $T_d$ ) at 5% weight loss was about 300°C, indicating it is thermally stable to be applied in PLEDs. Thermal transitional properties of **PSB** were studied by differential scanning calorimetric (DSC) measurements between -100°C and 260°C. A glass transition temperature ( $T_g$ ) was observed at about 20°C (inset), without detectable crystallization and melting transitions. Soft and bulky trihydroxy *tert*-butyl terminals give rise to low glass transition temperature. Moreover, these bulky terminals are effective in preventing regular molecular packing into crystallites, resulting in amorphous solid state.

The absorption and photoluminescence spectra of PSB in DMF solution ( $10^{-5}$  M) and as thin film spin-coated from DMF solution (10 mg/mL) are illustrated in **Figure 2**, with characteristic data summarized in **Table 1**. In DMF solution, PSB revealed three absorption peaks at 267, 307 and 342 nm, attributable to the hydroxyl groups  $n - \pi^*$  transition, pyrene and aryl groups  $\pi - \pi^*$  transition [24], and imine groups  $\pi - \pi^*$  transition [25], respectively. In film state, two absorptions at 294 nm and 430 nm were observed; the former is ascribed to blue shifted absorption of pyrene and aryl groups, while the latter is caused by the aggregation of PSB [26]. In DMF solution, PSB shows a weak emission peak at 515 nm (normalized), attributed to pyrene and aryl groups. However, no emission was detectable in film state, due probably to complete fluorescence quenching caused by the two terminal Schiff base (imine) groups. The fluorescence of excited pyrene groups is prohibited by photo-induced electron transfer (PET) from imine moieties [27]. Non-fluorescence of PSB is a great merit for electroluminescent devices, because its will not degrade color purity of the emissive layer when used as hole-buffer layer.

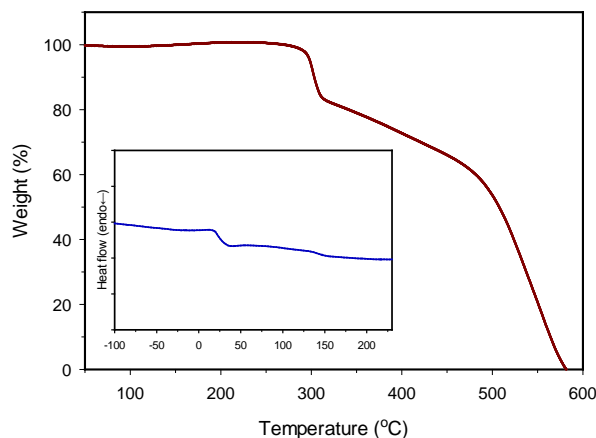


**Figure 1.** Thermogravimetric and differential scanning calorimetric (inset) traces of **PSB** at a heating rate of 10°C/min under nitrogen atmosphere.

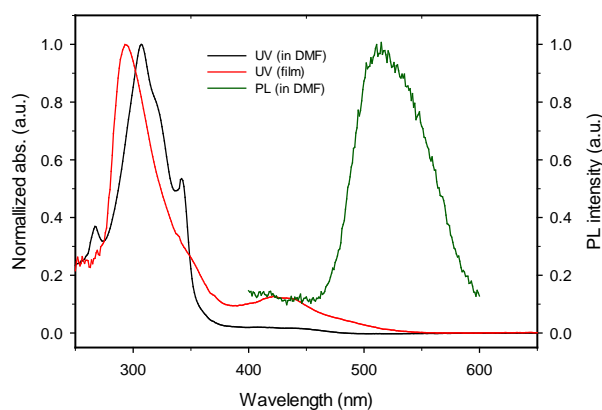


**Figure 2.** Normalized UV/Vis absorption and photoluminescence spectra of **PSB** in DMF solution and at film state.

**Table 1.** Optical properties of **PSB**.

	UV/vis $\lambda_{\max}$ (nm)		PL $\lambda_{\max}$ (nm) <sup>c</sup>		$E_g^m$ (eV) <sup>d</sup>
	solution <sup>a</sup>	film <sup>b</sup>	solution <sup>a</sup>	film <sup>b</sup>	
<b>PSB</b>	267,307,342	294,430	515	---	3.52

<sup>a</sup>In 10<sup>-5</sup> M DMF solution. <sup>b</sup>The film prepared by spin-coating 10 mg/mL in DMF solution on quartz substrate. <sup>c</sup>Excitation wavelength was 307 nm. <sup>d</sup>The value was estimated by the  $\lambda_{\text{onset}}$  of the UV/Vis spectrum.

Cyclic voltammetric analysis is a powerful method to evaluate electrochemical properties of organic and polymeric materials, especially the estimation of oxidation and reduction potentials. Usually the sample is coated onto the working electrode or dissolved in the electrolyte. The propensity to lose or obtain electron is readily estimated from the oxidation and reduction potentials. The **PSB** film was deposited onto the glassy carbon electrode by dropping its chloroform solution. The cyclic voltammogram of **PSB** is shown in **Figure 3** and the corresponding electrochemical data are summarized in **Table 2**. The CV curve was not a closed loop, probably attributed to the equilibrium between **PSB** and elec-

trolyte ions was still not established. The highest occupied molecular orbital (HOMO) and lowest unoccupied molecular orbital (LUMO) levels were estimated by

$$E_{\text{HOMO}} (\text{eV}) = -\left(E_{\text{onset(ox),FOC}} + 4.8\right)$$

$$\text{and } E_{\text{LUMO}} (\text{eV}) = -\left(E_{\text{onset(red),FOC}} + 4.8\right)$$

where  $E_{\text{onset(ox),FOC}}$  and  $E_{\text{onset(red),FOC}}$  are the onset oxidation and onset reduction potentials respectively, relative to the ferrocene/ferrocenium couple whose energy level is already known ( $-4.8$  eV). The estimated LUMO and HOMO energy levels are  $-2.55$  eV and  $-6.33$  eV, respectively. Therefore, the electrochemically determined band-gap ( $E_{\text{g}}^{\text{el}}$ ) is  $3.78$  eV. The estimated LUMO and HOMO levels of **PSB** are much lower than those of pyrene ( $-1.48$  eV,  $-5.44$  eV) [28], due to the presence of two terminal Schiff base-modified phenol groups. Low HOMO level is effective in reducing hole mobility, which in turn raise carriers' recombination ratio in the emissive layer (Super Yellow) to enhance emission efficiency. Density functional theory (DFT) theory was employed to investigate electron distribution in **PSB**, using an electronic structure-modeling program Gaussian 09. As shown in **Figure 4**, the HOMO is exclusively localized on pyrene core, while the LUMO is mainly located on the Schiff base groups and partially on the pyrene core. Therefore, the two Schiff base groups in **PSB** should be effective in reducing hole mobility due to their electron-withdrawing characteristics.

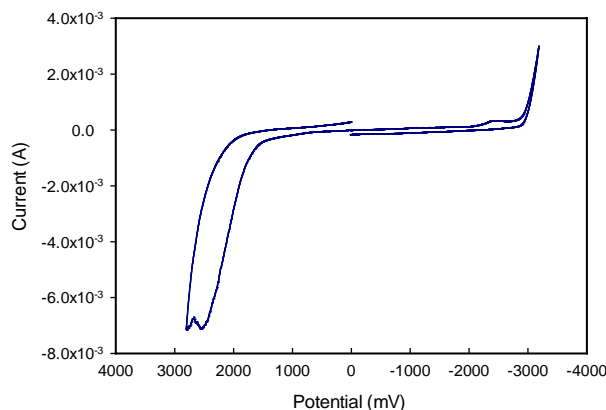


**Figure 3.** Cyclic voltammogram of PSB coated on carbon electrode, measured in  $0.1$  M (n-Bu)  $4\text{NClO}_4$ ; scan rate:  $100$  mV/s.

**Table 2.** Electrochemical properties of PSB and pyrene.

	$E_{\text{onset(ox) vs.FOC}}$ (V) <sup>a</sup>	$E_{\text{onset(red) vs.FOC}}$ (V) <sup>a</sup>	$E_{\text{HOMO}}$ (eV) <sup>b</sup>	$E_{\text{LUMO}}$ (eV) <sup>c</sup>	$E_{\text{g}}^{\text{el}}$ (eV) <sup>d</sup>
<b>PSB</b>	1.53	-2.25	-6.33	-2.55	3.78
Pyrene [30]	---	---	-5.44	-1.48	3.86

<sup>a</sup> $E_{\text{FOC}} = 0.08$  V versus Ag/AgNO<sub>3</sub>, <sup>b</sup> $E_{\text{HOMO}} = -(E_{\text{onset(ox),FOC}} + 4.8)$  eV. <sup>c</sup> $E_{\text{LUMO}} = -(E_{\text{onset(red),FOC}} + 4.8)$  eV. <sup>d</sup> $E_{\text{g}} = |\text{LUMO-HOMO}|$ eV.

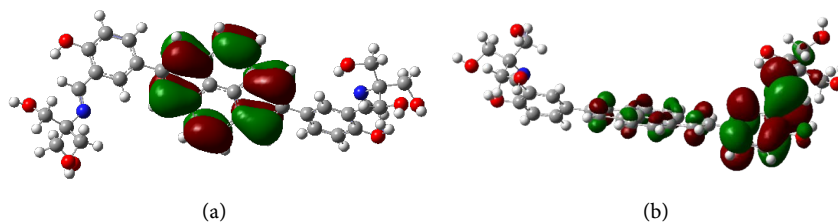


**Figure 4.** (a) HOMO and (b) LUMO distributions of PSB calculated by Gaussian 09 software [DFT-B3LYP/6-311G(d) level].

**Figure 5** shows the energy level diagrams of hole-buffering and hole-blocking devices. The HOMO level of BCP ( $-6.7$  eV) is much lower than  $-5.0$  eV of the emissive SY layer. Accordingly, BCP is effective in blocking the holes when inserted between emissive SY layer and the cathode. On the other hand, the HOMO level of **PSB** ( $-6.33$  eV) is also much lower than  $-5.0$  eV of the hole-injecting PEDOT:PSS layer. By the same way, **PSB** can effectively obstruct the holes when inserted between PEDOT:PSS and emissive SY layers. This will reduce transport rate of the holes to raise carrier recombination ratio and emission efficiency, because for most conjugated emissive materials holes transport much faster than electrons [29].

### 3.2. Surface Morphology

Surface morphology of deposited film during device fabrication was observed by an atomic force microscopy (AFM); the root-mean-square (rms) surface roughness was estimated from the AFM topography images. At first, the effect of concentration was investigated using **PSB** solutions in DMF (5, 10, 15 and 20 mg/mL). The hole-injecting PEDOT:PSS was spin-coated onto ITO substrate at 3000 rpm followed by annealing at  $140^{\circ}\text{C}$  for 20 min. The **PSB** was then spin-coated on top of the PEDOT:PSS layer first at 2000 rpm for 15 sec and then at 6000 rpm for 1 min. The spin-coated **PSB** film was annealed at  $70^{\circ}\text{C}$  for 20 min under nitrogen atmosphere. **Figure 6** shows the AFM topography images. The root-mean-square (rms) surface roughness of the PEDOT:PSS layer was 1.18 nm which is comparable to that reported in literature. **PSB** films revealed smooth morphology when spin-coated from lower concentrations (5 and 10 mg/mL), with surface roughness of 1.88 nm and 2.08 nm, respectively. However, the surface became much rougher when spin-coated from higher concentrations (15 and 20 mg/mL), with the roughness of 10.70 nm and 9.77 nm, respectively.

### 3.3. Electroluminescent Properties

To investigate the feasibility of **PSB** as a hole-buffering material, multilayer PLED devices were fabricated [ITO/PEDOT:PSS (40 nm)/**PSB** (x nm)/SY (70 nm)/LiF (1 nm)/Al (90 nm)] and their optoelectronic characteristics measured. For comparative study, multilayer blank PLED device without the **PSB** layer [ITO/PEDOT:PSS (40 nm)/SY (70 nm)/LiF (1 nm)/Al (90 nm)] was also fabricated. Moreover, the device with conventional BCP as a hole-blocking layer

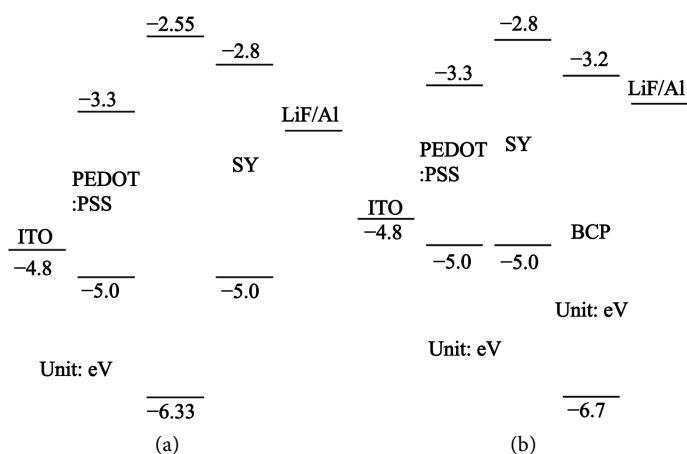


**Figure 5.** Energy level diagrams of the PLEDs using (a) PSB as hole-buffering layer and (b) BCP as hole-blocking layer.

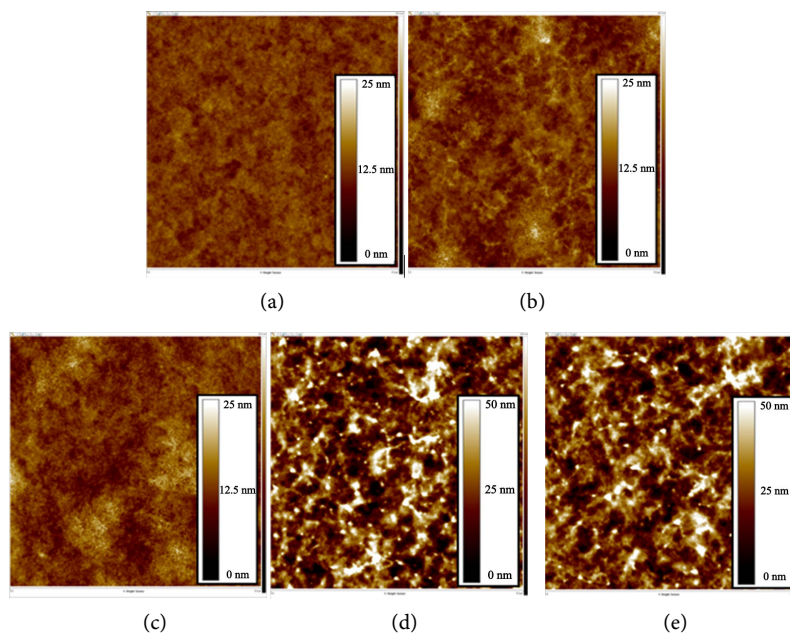


**Figure 6.** AFM images of (a) PEDOT:PSS film on top of ITO and PSB on top of the PEDOT:PSS film coated from different concentration; (b) 5 mg/mL; (c) 10 mg/mL; (d) 15 mg/mL; (e) 20 mg/mL.

[ITO/PEDOT:PSS (40 nm)/SY (70 nm)/BCP (15 nm)/LiF (1 nm)/Al (90 nm)] was also prepared to evaluate the effectiveness of hole-buffering **PSB**. **Figure 7** demonstrates luminance and current density versus voltage and efficiency versus current density of the multilayer devices, with the characteristic data summarized in **Table 3**. The hole-buffer layer was inserted between hole-injecting PEDOT:PSS and emissive SY layers by spin-coating **PSB** solutions with different concentrations (5, 7, 10, 15, 20 mg/mL). The thickness of deposited **PSB** films was increased gradually from 7 nm to 38 nm with the concentration increasing from 5 mg/mL to 20 mg/mL (**Table 3**).

As expected, insertion of hole-blocking BCP layer (15 nm) decreases current

density moderately under the same operating voltages (**Figure 7(b)**); for instance, the current density of blank device was about 200 mA/cm<sup>2</sup> at 8 V which decreased to *ca.* 100 mA/cm<sup>2</sup> after the insertion of BCP. The BCP layer effectively blocks the holes at the interface with the emissive SY layer. However, hole-buffering **PSB** layer reduced the current density dramatically, with the reduction increased with thickness. In addition, the maximum luminance of **PSB**-based device increased significantly from 9060 cd/m<sup>2</sup> to 26,439 cd/m<sup>2</sup> as the thickness increased from 7 nm to 15 nm (**Table 3**). Apparently, the maximum luminance (26,439 cd/m<sup>2</sup>) at 15 nm **PSB** is much higher than 9802 cd/m<sup>2</sup> and 15,496 cd/m<sup>2</sup> of the blank and BCP-based devices, respectively. However, the maximum luminance dropped dramatically to 8103 cd/m<sup>2</sup> and 5812 cd/m<sup>2</sup> when the thickness of **PSB** further increased to 24 nm and 38 nm respectively. Clearly, an optimal **PSB** thickness exists at about 15 nm, at which the balance of carriers is most effective.

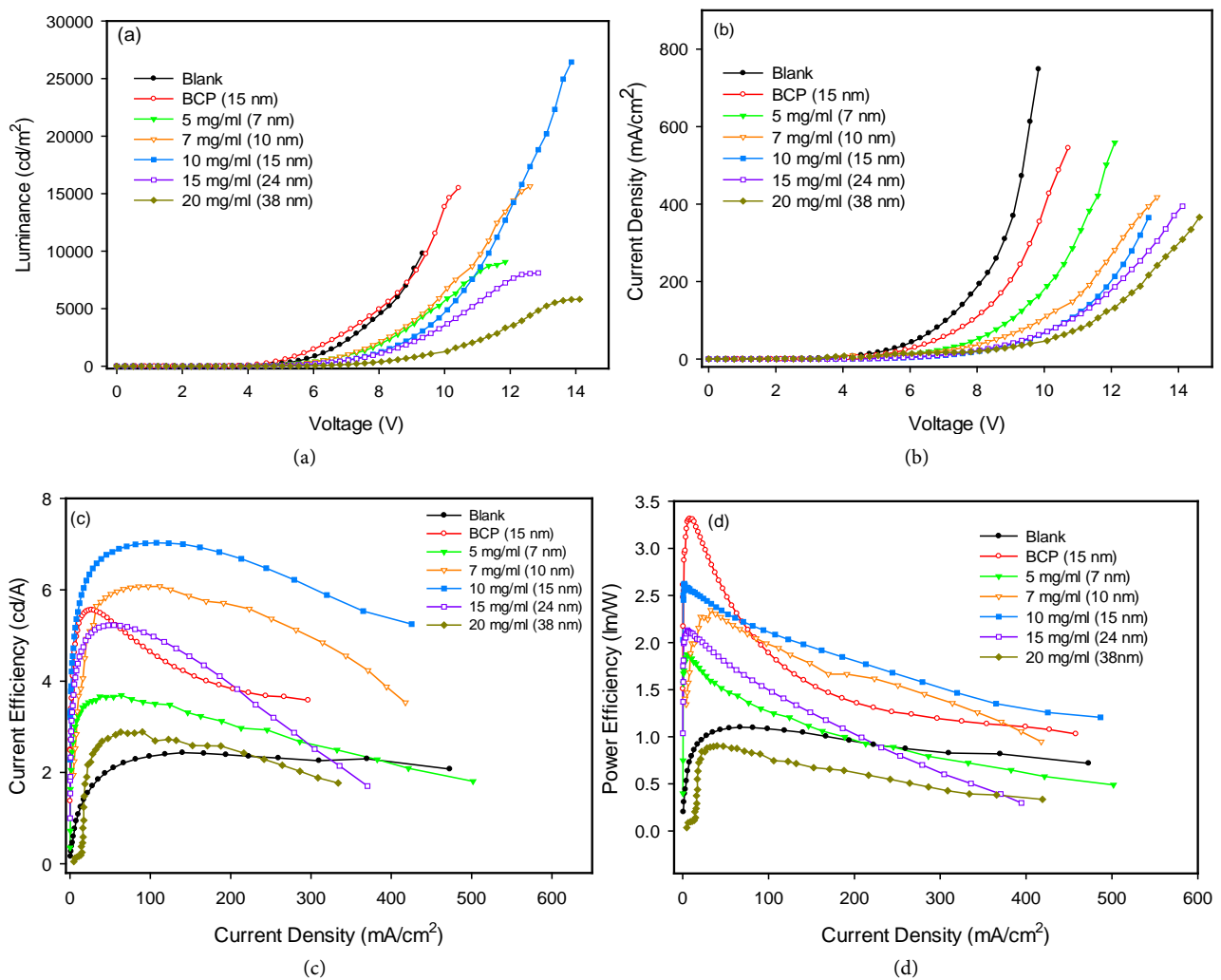


**Figure 7.** (a) Luminance versus voltage; (b) current density versus voltage; (c) current efficiency versus current density and (d) power efficiency versus current density characteristics of the OLEDs using PSB as hole-buffer layer. Device structure: ITO/PEDOT:PSS/PSB(x nm)/SY/(BCP)/LiF/Al.

**Table 3.** Electroluminescent properties of multilayer PLEDs.<sup>a</sup>

	Thickness <sup>b</sup>	V <sub>on</sub> <sup>c</sup>	I <sub>max</sub> <sup>d</sup>	CE <sub>max</sub> <sup>e</sup>	PE <sub>max</sub> <sup>f</sup>	CIE <sup>g</sup>
	(nm)	(V)	(cd/m <sup>2</sup> )	(cd/A)	(lm/W)	(x, y)
Blank	---	3.3	9802	2.43	1.10	(0.40, 0.58)
BCP	15	3.3	15,496	5.56	3.31	(0.42, 0.57)
5 mg/mL <sup>h</sup>	7	3.5	9060	3.69	1.87	(0.44, 0.55)
7 mg/mL <sup>h</sup>	10	3.7	15,640	6.08	2.30	(0.45, 0.54)
10 mg/mL <sup>h</sup>	15	3.9	26,439	7.03	2.62	(0.46, 0.52)
15 mg/mL <sup>h</sup>	24	4.0	8103	5.26	2.13	(0.46, 0.53)
20 mg/mL <sup>h</sup>	38	4.9	5812	2.89	0.90	(0.46, 0.53)

<sup>a</sup>Device structure: ITO/PEDOT:PSS (40 nm)/**PSB** (x nm)/SY (70 nm)/[BCP (15 nm)]/LiF (1 nm)/Al (90 nm). <sup>b</sup>Thickness was determined by alpha-step measurement. <sup>c</sup>Turn-on voltage at 10 cd/m<sup>2</sup>. <sup>d</sup>Maximum luminance. <sup>e</sup>Maximum current efficiency. <sup>f</sup>Maximum power efficiency. <sup>g</sup>The 1931 CIE coordinate at maximum current efficiency. <sup>h</sup>Concentration of **PSB** in DMF.

Similar trends are observed for current efficiency and power efficiency as shown in **Figure 7(c)** and **Figure 7(d)** and **Table 3**. The maximum current efficiency first increased from 3.69 cd/A to 7.03 cd/A, followed with dramatic drop to 5.26 and 2.89 cd/A at 24 nm and 38 nm, respectively. However, these current efficiencies are still higher than 2.43 cd/A of the blank device. Furthermore, hole-buffering **PSB** is more effective than hole-blocking BCP in enhancing efficiency. Under the same thickness (15 nm), the current efficiency of **PSB**-based device was 7.03 cd/A, compared with 5.56 cd/A of BCP-based one. But the **PSB** layer raised turn-on voltage gradually from 3.3 V to 4.9 V when its thickness was increased from 7 nm to 38 nm. Apparently, inserting hole-buffering **PSB** results in significant performance enhancement, in terms of maximum luminance and current efficiency, compared with blank device (**Table 3**). The performance is even superior to the device with conventional BCP as the hole-blocking layer (maximum luminance: 15,496 cd/m<sup>2</sup>, maximum current efficiency: 5.56 cd/A). These results indicate that hole-buffering **PSB** outperforms hole-blocking BCP when applied to balance carriers' recombination. Single-carrier transporting devices are thought effective in elucidating underlying mechanisms, whose discussion is in the next section.

Single-carrier devices (hole-only and electron-only) with hole-buffering (**PSB**) or hole-blocking (**BCP**) layers were fabricated to investigate charge-transporting properties. The hole-only device used Au as cathode to replace LiF/Al, whereas the electron-only one employed ZnO to replace hole-injecting PEDOT:PSS. For hole-only device, large barrier height between Au (work function: 5.1 eV) and emissive SY layer (LUMO: -2.8 eV) obstructs electron injection, resulting in exclusive holes' contribution to current density. Similarly, for electron-only device, the barrier height between ZnO (-7.6 eV) and ITO anode (-4.8 eV) is very high (2.8 eV), leading to exclusive contribution of electrons. Therefore, the current density of hole-only and electron-only devices can be seen as hole density and electron density. For hole-only devices (**Figure 8(a)**), current density reduced

dramatically with 7 nm **PSB** or 15 nm BCP as hole-buffering or hole-blocking layer. Moreover, the reduction increased gradually with increasing thickness of **PSB** (from 7 nm to 38 nm).

On the contrary, for electron-only devices the current density increased only slightly with **PSB** thickness (from 7 nm to 15 nm) as shown in **Figure 8(b)**. Further increase to 24 nm and 38 nm the current density became lower than the blank device. However, the BCP layer (15 nm) raised the current density significantly. This is because BCP, inserted between emissive SY and Al cathode, is also an effective electron injection/transport material due to its low LUMO level ( $-3.2$  eV), in addition to its hole-blocking capability (low HOMO level). The **PSB** layer, inserted between emissive SY and ZnO, promotes electron transport slightly at low thickness (7 - 15 nm) due probably to polar and electron-withdrawing imine and trihydroxy *tert*-butyl groups. Interfacial polarization in carrier-transporting layer contributes greatly to the promotion of carriers' injection. However, the contribution gradually diminishes with increasing thickness due to decreased polarity gradient.

The results indicate both **PSB** and BCP reduce transport rate of the holes to enhance carrier balance and device performance. Moreover, The **PSB** is inserted between hole-injecting PEDOT:PSS and emitting SY layers to reduce hole's transport into SY layer. This leads to more homogeneous distribution of the excitons formed in the SY layer. However, the BCP layer is inserted between the emitting SY layer and the LiF/Al cathode to block the holes from quenching at the cathode. This blocking accumulates a large amount of the holes in a narrow region near the interface between the emitting SY and BCP layers. Therefore, the distribution of the excitons in emitting SY layer is very different for **PSB** and BCP devices. As shown in **Figure 9(a)**, the recombination region for BCP-based device is narrow and close to the interface of the emitting SY and BCP layers. On the contrary, recombination region for **PSB** device should be much more

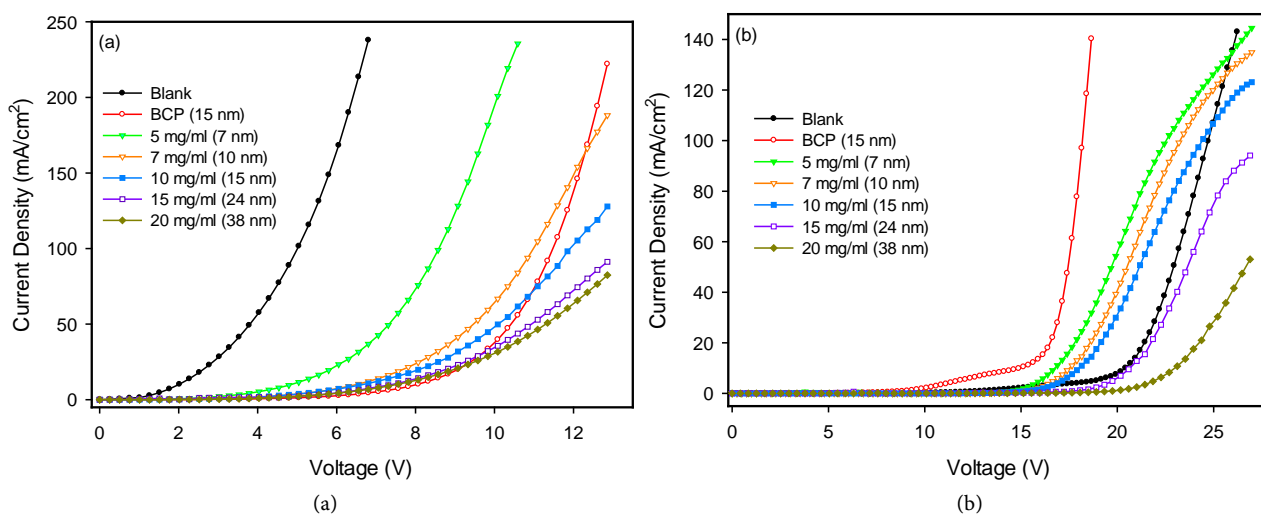


**Figure 8.** Current density versus voltage characteristics of (a) hole-only and (b) electron-only EL devices. Devices structure: (a) HOD: ITO/PEDOT:PSS/PSB (x nm)/SY/(BCP)/Au; (b) EOD: ITO/ZnO/PSB (x nm)/SY/(BCP)/LiF/Al.

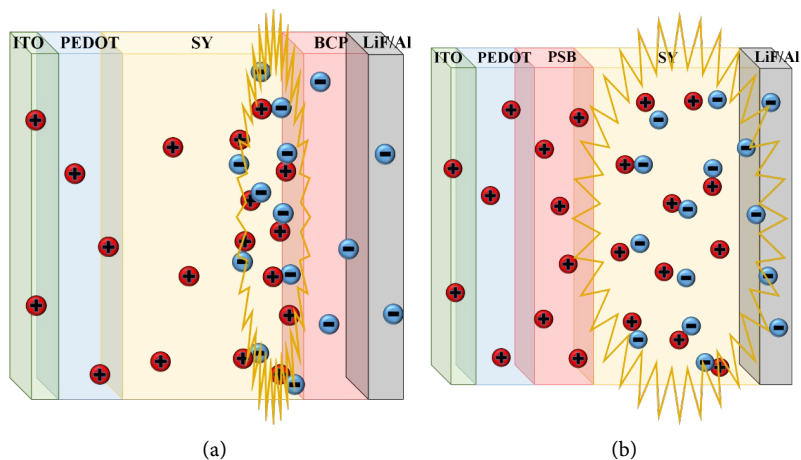


**Figure 9.** Proposed illustrations for recombination region of holes and electrons in the PLEDs using (a) hole-blocking layer (BCP) and (b) hole-buffer layer (PSB).

homogeneous and broader (**Figure 9(b)**). Broader charges recombination region usually results higher charges' recombination ratio and device performance [30] [31] [32].

#### 4. Conclusion

We have successfully synthesized a new compound **PSB** composed of pyrene core linked with trihydroxy *tert*-butyl groups through imine moiety by the Suzuki-coupling reaction and applied as hole-buffer layer in multilayer PLEDs. Thermal decomposition temperature ( $T_d$ ) at 5% weight loss was observed at 300°C. The HOMO and LUMO levels of **PSB** were  $-6.33$  and  $-2.55$  eV respectively, estimated from onset oxidation and reduction potentials determined by cyclic voltammetry. Multilayer PLEDs have been successfully fabricated (ITO/PEDOT:PSS/**PSB**/SY/LiF/Al), in which PEDOT:PSS, **PSB** and SY layers were deposited by spin-coating process. The thickness of **PSB** layer increased gradually from 7 nm to 38 nm with **PSB** concentration increased from 5 mg/mL to 20 mg/mL in DMF. Inserting **PSB** as hole-buffer layer effectively raised luminance and emission efficiency, with optimal **PSB** thickness being 15 nm. The maximum luminance and maximum current efficiency were 26,439 cd/m<sup>2</sup> and 7.03 cd/A, respectively, which were superior to 9802 cd/m<sup>2</sup> and 2.43 cd/A of the blank device. Under the same thickness (15 nm), the **PSB**-based device also outperformed the one with the conventional BCP as hole-blocking layer [ITO/PEDOT:PSS/SY/BCP/LiF/Al], in terms of maximum luminance and maximum current efficiency (15,496 cd/m<sup>2</sup>, 5.56 cd/A). Current results indicate that the **PSB** composed of pyrene, polar imine and trihydroxy *tert*-butyl groups is highly effective in buffering holes' transport to enhance performance of electro-luminescent devices.

#### Acknowledgements

Authors are thankful to the Ministry of Science and Technology (MOST) of

Taiwan for financial support through grant MOST105-2221-E-006-250.

## References

- [1] Burroughes, J., Bradley, D., Brown, A., Marks, R., Mackay, K., Friend, R., Burns, P. and Holmes, A. (1990) Light-Emitting Diodes Based on Conjugated Polymers. *Nature*, **347**, 539-541. <https://doi.org/10.1038/347539a0>
- [2] Burrows, P.E., Graff, G.L., Gross, M.E., Martin, P.M., Shi, M.-K., Hall, M., Mast, E., Bonham, C., Bennett, W. and Sullivan, M.B. (2001) Ultra Barrier Flexible Substrates for Flat Panel Displays. *Displays*, **22**, 65-69. [https://doi.org/10.1016/S0141-9382\(00\)00064-0](https://doi.org/10.1016/S0141-9382(00)00064-0)
- [3] Sugimoto, A., Ochi, H., Fujimura, S., Yoshida, A., Miyadera, T. and Tsuchida, M. (2004) Flexible OLED Displays Using Plastic Substrates. *IEEE Journal of Selected Topics in Quantum Electronics*, **10**, 107-114. <https://doi.org/10.1109/JSTQE.2004.824112>
- [4] Qiu, Y., Gao, Y., Wei, P. and Wang, L. (2002) Organic Light-Emitting Diodes with Improved Hole-Electron Balance by Using Copper Phthalocyanine/Aromatic Diamine Multiple Quantum Wells. *Applied Physics Letters*, **80**, 2628-2630. <https://doi.org/10.1063/1.1468894>
- [5] Yin, S., Yi, Y., Li, Q., Yu, G., Liu, Y. and Shuai, Z. (2006) Balanced Carrier Transports of Electrons and Holes in Silole-Based Compounds—A Theoretical Study. *Journal of Physical Chemistry A*, **110**, 7138-7143. <https://doi.org/10.1021/jp057291o>
- [6] Yamashita, Y. (2009) Organic Semiconductors for Organic Field-Effect Transistors. *Science and Technology of Advanced Materials*, **10**, Article ID: 024313. <https://doi.org/10.1088/1468-6996/10/2/024313>
- [7] Hung, L., Tang, C.W. and Mason, M.G. (1997) Enhanced Electron Injection in Organic Electroluminescence Devices Using an Al/LiF Electrode. *Applied Physics Letters*, **70**, 152-154. <https://doi.org/10.1063/1.118344>
- [8] Brown, T., Kim, J., Friend, R., Cacialli, F., Daik, R. and Feast, W. (1999) Built-In Field Electroabsorption Spectroscopy of Polymer Light-Emitting Diodes Incorporating a Doped Poly (3, 4-Ethylene Dioxythiophene) Hole Injection Layer. *Applied Physics Letters*, **75**, 1679-1681. <https://doi.org/10.1063/1.124789>
- [9] Adamovich, V.I., Cordero, S.R., Djurovich, P.I., Tamayo, A., Thompson, M.E., D'Andrade, B.W. and Forrest, S.R. (2003) New Charge-Carrier Blocking Materials for High Efficiency OLEDs. *Organic Electronics*, **4**, 77-87. <https://doi.org/10.1016/j.orgel.2003.08.003>
- [10] Lin, W.C., Lin, H.W., Mondal, E. and Wong, K.T. (2015) Efficient Solution-Processed Green and White Phosphorescence Organic Light-Emitting Diodes Based on Bipolar Host Materials. *Organic Electronics*, **17**, 1-8. <https://doi.org/10.1016/j.orgel.2014.11.002>
- [11] Gao, H., Qin, C., Zhang, H., Wu, S., Su, Z.M. and Wang, Y. (2008) Theoretical Characterization of a Typical Hole/Exciton-Blocking Material Bathocuproine and Its Analogues. *Journal of Physical Chemistry A*, **112**, 9097-9103. <https://doi.org/10.1021/jp804308e>
- [12] Ikai, M., Tokito, S., Sakamoto, Y., Suzuki, T. and Taga, Y. (2001) Highly Efficient Phosphorescence from Organic Light-Emitting Devices with an Exciton-Block Layer. *Applied Physics Letters*, **79**, 156-158. <https://doi.org/10.1063/1.1385182>
- [13] Su, H.-C. and Hsu, J.-H. (2015) Improving the Carrier Balance of Light-Emitting Electrochemical Cells Based on Ionic Transition Metal Complexes. *Dalton Transactions*

- tions, **44**, 8330-8345. <https://doi.org/10.1039/C4DT01675K>
- [14] Xia, Y.-J., Lin, J., Tang, C., Yin, K., Zhong, G.-Y., Ni, G., Peng, B., Gan, F.-X. and Huang, W. (2006) High-Efficiency Blue-Emitting Organic Light-Emitting Devices with 4, 4', 4''-Tris (N-Carbazolyl)-Triphenylamine as the Hole/Exciton-Blocking Layer. *Journal of Physics D: Applied Physics*, **39**, 4987. <https://doi.org/10.1088/0022-3727/39/23/013>
- [15] Tadayyon, S.M., Grandin, H.M., Griffiths, K., Norton, P.R., Aziz, H. and Popovic, Z.D. (2004) CuPc Buffer Layer Role in OLED Performance: A Study of the Interfacial Band Energies. *Organic Electronics*, **5**, 157-166. <https://doi.org/10.1016/j.orgel.2003.10.001>
- [16] Chou, S.-Y. and Chen, Y. (2016) Hole-Buffer Polymer Composed of Alternating *p*-Terphenyl and Tetraethylene Glycol Ether Moieties: Synthesis and Application in Polymer Light-Emitting Diodes. *Journal of Polymer Science Part A: Polymer Chemistry*, **54**, 785-794. <https://doi.org/10.1002/pola.27911>
- [17] Lee, S.J., Lee, S.E., Lee, D.H., Koo, J.R., Lee, H.W., Yoon, S.S., Park, J. and Kim, Y.K. (2014) Effect of Broad Recombination Zone in Multiple Quantum Well Structures on Lifetime and Efficiency of Blue Organic Light-Emitting Diodes. *Japanese Journal of Applied Physics*, **53**, Article ID: 101601. <https://doi.org/10.7567/JJAP.53.101601>
- [18] Forsythe, E., Abkowitz, M. and Gao, Y. (2000) Tuning the Carrier Injection Efficiency for Organic Light-Emitting Diodes. *Journal of Physical Chemistry B*, **104**, 3948-3952. <https://doi.org/10.1021/jp993793o>
- [19] Shibata, M., Sakai, Y. and Yokoyama, D. (2015) Advantages and Disadvantages of Vacuum-Deposited and Spin-Coated Amorphous Organic Semiconductor Films for Organic Light-Emitting Diodes. *Journal of Materials Chemistry C*, **3**, 11178-11191. <https://doi.org/10.1039/C5TC01911G>
- [20] Duan, L., Hou, L., Lee, T.-W., Qiao, J., Zhang, D., Dong, G., Wang, L. and Qiu, Y. (2010) Solution Processable Small Molecules for Organic Light-Emitting Diodes. *Journal of Materials Chemistry*, **20**, 6392-6407. <https://doi.org/10.1039/b926348a>
- [21] Otsubo, T., Aso, Y. and Takimiya, K. (2002) Functional Oligothiophenes as Advanced Molecular Electronic Materials. *Journal of Materials Chemistry*, **12**, 2565-2575. <https://doi.org/10.1039/b203780g>
- [22] Ferguson, J. (1958) Absorption and Fluorescence Spectra of Crystalline Pyrene. *Journal of Chemical Physics*, **28**, 765-768. <https://doi.org/10.1063/1.1744267>
- [23] Hsu, P.-F. and Chen, Y. (2018) Synthesis of a Pyrene-Derived Schiff Base and Its Selective Fluorescent Enhancement by Zinc and Aluminum Ions. *International Journal of Organic Chemistry*.
- [24] Qiao, Y.L., Zhang, J., Xu, W. and Zhu, D.B. (2011) Novel 2,7-Substituted Pyrene Derivatives: Syntheses, Solid-State Structures, and Properties. *Tetrahedron*, **67**, 3395-3405. <https://doi.org/10.1016/j.tet.2011.03.055>
- [25] Rathfon, J.M., AL-Badri, Z.M., Shunmugam, R., Berry, S.M., Pabba, S., Keynton, R.S., Cohn, R.W. and Tew, G.N. (2009) Fluorimetric Nerve Gas Sensing Based on Pyrene Imines Incorporated into Films and Sub-Micrometer Fibers. *Advanced Functional Materials*, **19**, 689-695. <https://doi.org/10.1002/adfm.200800947>
- [26] Ou, C.J., Lei, Z.F., Sun, M.L., Xie, L.H., Qian, Y., Zhang, X.W. and Huang, W. (2015) Dumbbell Effects of Solution-Processed Pyrene-Based Organic Semiconductors on Electronic Structure, Morphology and Electroluminescence. *Synthetic Metals*, **200**, 135-142. <https://doi.org/10.1016/j.synthmet.2014.12.034>
- [27] Hsieh, W.H., Wan, C.F., Liao, D.J. and Wu, A.T. (2012) A Turn-On Schiff Base Fluorescence Sensor for Zinc Ion. *Tetrahedron Letters*, **53**, 5848-5851.

<https://doi.org/10.1016/j.tetlet.2012.08.058>

- [28] Chercka, D., Yoo, S.J., Baumgarten, M., Kim, J.J. and Mullen, K. (2014) Pyrene Based Materials for Exceptionally Deep Blue OLEDs. *Journal of Materials Chemistry C*, **2**, 9083-9086. <https://doi.org/10.1039/C4TC01801J>
- [29] Wang, B.C., Chang, J.C., Tso, H.C., Hsu, H.F. and Cheng, C.Y. (2003) Theoretical Investigation the Electroluminescence Characteristics of Pyrene and Its Derivatives. *Journal of Molecular Structure: THEOCHEM*, **629**, 11-20. [https://doi.org/10.1016/S0166-1280\(02\)00787-X](https://doi.org/10.1016/S0166-1280(02)00787-X)
- [30] Malliaras, G.G. and Scott, J.C. (1998) The Roles of Injection and Mobility in Organic Light Emitting Diodes. *Journal of Applied Physics*, **83**, 5399-5403. <https://doi.org/10.1063/1.367369>
- [31] Liao, C.T., Chen, H.F., Su, H.C. and Wong, K.T. (2011) Tailoring Balance of Carrier Mobilities in Solid-State Light-Emitting Electrochemical Cells by Doping a Carrier Trapper to Enhance Device Efficiencies. *Journal of Materials Chemistry*, **21**, 17855-17862. <https://doi.org/10.1039/c1jm13245h>
- [32] Lee, S.E., Lee, H.W., Lee, J.W., Hwang, K.M., Park, S.N., Yoon, S.S. and Kim, Y.K. (2015) Optimization of Hybrid Blue Organic Light-Emitting Diodes Based on Singlet and Triplet Exciton Diffusion Length. *Japanese Journal of Applied Physics*, **54**, Article ID: 06FG09. <https://doi.org/10.7567/JJAP.54.06FG09>